# Temperature Dependence of the Quantum Yields for the Photolysis of $NO_2$ near the Dissociation Limit

**Coleen M. Roehl,† John J. Orlando,* Geoffrey S. Tyndall, Richard E. Shetter, Gabriel J. Vázquez,‡ Christopher A. Cantrell, and Jack G. Calvert**

*Atmospheric Chemistry Division, National Center for Atmospheric Research, Boulder, Colorado 80303*

*Received: February 23, 1994; In Final Form: May 16, 1994•*

Photolysis quantum yields for $NO_2 + h\nu \rightarrow O(^3P) + NO$ are reported for the wavelength range 388–411 nm at two temperatures (248 and 298 K). At room temperature, the quantum yield is found to be (0.93 ± 0.10) from 388 to 398 nm and to decrease smoothly to a value of 0.12 at 411 nm. Beyond the dissociation threshold (397.9 nm), quantum yields obtained at 248 K are found to be significantly lower than those at 298 K (by ≈10% at 400 nm and ≈50% at 411 nm). The observed quantum yield data beyond the thermodynamic threshold are explained quantitatively in terms of a mechanism involving both direct dissociation (through the use of internal rovibrational energy) and dissociation of excited $NO_2$ induced by collisions with the bath gas.

## Introduction

The photochemistry of nitrogen dioxide, $NO_2$, has been studied in the UV/visible regions of the spectrum for more than half a century,[1-46] yet a sound quantitative understanding of its photochemistry near the photodissociation threshold has not been achieved. Photolysis is the dominant loss process for $NO_2$ in the troposphere and is the major source of tropospheric $O_3$:

$$NO_2 + h\nu \rightarrow O(^3P) + NO \quad (1)$$

$$O(^3P) + O_2 + M \rightarrow O_3 + M \quad (2)$$

Because NO is oxidized back to $NO_2$,

$$O_3 + NO \rightarrow O_2 + NO_2 \quad (3)$$

$$RO_2 + NO \rightarrow RO + NO_2 \quad (4)$$

a "photostationary state" is established in which the concentration of $O_3$ is determined by the ratio of the concentrations of $NO_2$ and NO and by the rates of reactions 1–4:

$$[O_3] = \frac{\frac{j_1[NO_2]}{[NO]} - k_4[RO_2]}{k_3} \quad (A)$$

Here, $j_1$ is the first-order rate for reaction 1, $k_3$ is the second-order rate constant for reaction 3, and $k_4$ is a generalized second-order rate constant for the reaction of peroxy radicals ($HO_2$ and $RO_2$, where R refers to an alkyl or acyl radical) with NO. Because of its primary importance in controlling tropospheric ozone, an accurate parameterization of the $NO_2$ photodissociative process is imperative for atmospheric modeling.

The atmospheric photolysis rate $j_1$ has been extensively studied both in field experiments and in the laboratory.[20-25,44-46] Direct field measurements of $j_1$ have been conducted at specific locations through the use of actinometers or radiometers. In the laboratory studies, the absorption cross sections, $\sigma(\lambda,T)$, and quantum yields, $\phi(\lambda,T)$, are measured as a function of temperature and wavelength and are then combined with tabulated actinic fluxes, $I(\lambda,\chi)$, as a function of wavelength and solar zenith angle, to determine $j_1$:

$$j(NO_2) = \int \sigma(\lambda,T)\, \phi(\lambda,T)\, I(\lambda,\chi)\, d\lambda \quad (B)$$

Absorption cross sections for $NO_2$ have been studied by numerous authors.[8,9,29-43] The absorption feature of interest extends from about 250 to 650 nm and consists of substantial fine structure superimposed on a broad continuum. The complexity of the spectrum is attributed to strong mixing of the excited states ($^2B_1$ and $^2B_2$) with the electronic ground state ($^2A_1$). Because of the structured nature of the spectral features, absorption cross sections and their temperature dependence vary with spectral resolution.

A number of studies of $NO_2$ quantum yields have been reported at 298 K.[1-10] Quantum yields are near unity at wavelengths up to and slightly beyond the dissociation limit of 397.9 nm[26,27] and then rapidly decrease to near zero at ~425 nm. The data between 360 and 400 nm are very scattered, with differences of as much as 60% at some wavelengths. The currently recommended quantum yield data at room temperature are taken from the work of Gardner *et al.*[10]

Temperature-dependent quantum yields have been measured mostly at one wavelength, 404.7 nm.[5,9,10] In general, a smooth increase in quantum yield with increasing temperature has been observed with quantum yields increasing from about 0.25 at 225 K to about 0.7 at 500 K. Davenport[9] has also measured $NO_2$ quantum yields at low temperature (223 K) at selected wavelengths between 390 and 420 nm. A decrease in the quantum yield with decreasing temperature was observed for wavelengths of 400 nm or longer.

It has long been recognized that $NO_2$ dissociation occurs at wavelengths longer than the thermodynamic dissociation limit (397.9 nm). Pitts *et al.*[5] first addressed this issue when they reported a marked temperature effect on quantum yields measured at 404.7 nm. They proposed that the unexpected dissociation of $NO_2$ was due to internal rotational energy of the $NO_2$ molecules. Subsequent reports,[6,10,14] based on the original hypothesis of Pitts *et al.*, have shown that the experimental quantum yields are significantly higher than the calculated ones, even if it is assumed that all rovibrational energy can be used in the photodissociation process. In an attempt to resolve the discrepancy between observed and calculated quantum yields, Calvert *et al.*[28] postulated that larger absorption cross sections for vibrationally excited $NO_2$ ($\sigma_v$) relative to vibrationless $NO_2$ ($\sigma_o$) could enhance $NO_2$ quantum yields, despite the small populations of vibrationally excited states. However, $NO_2$ absorption cross sections measured at low resolution (1.5 nm) between 233 and 397 K[29] indicated that $\sigma_v < \sigma_o$ at 404.7 nm, in conflict with the results of Calvert *et al.*[28]

* Author to whom correspondence should be addressed.
† Currently at the Max-Planck-Institut für Chemie, Mainz, Germany 55020.
‡ On sabbatical leave from Instituto de Física, UNAM, México.
• Abstract published in *Advance ACS Abstracts*, July 15, 1994.

0022-3654/94/2098-7837$04.50/0 

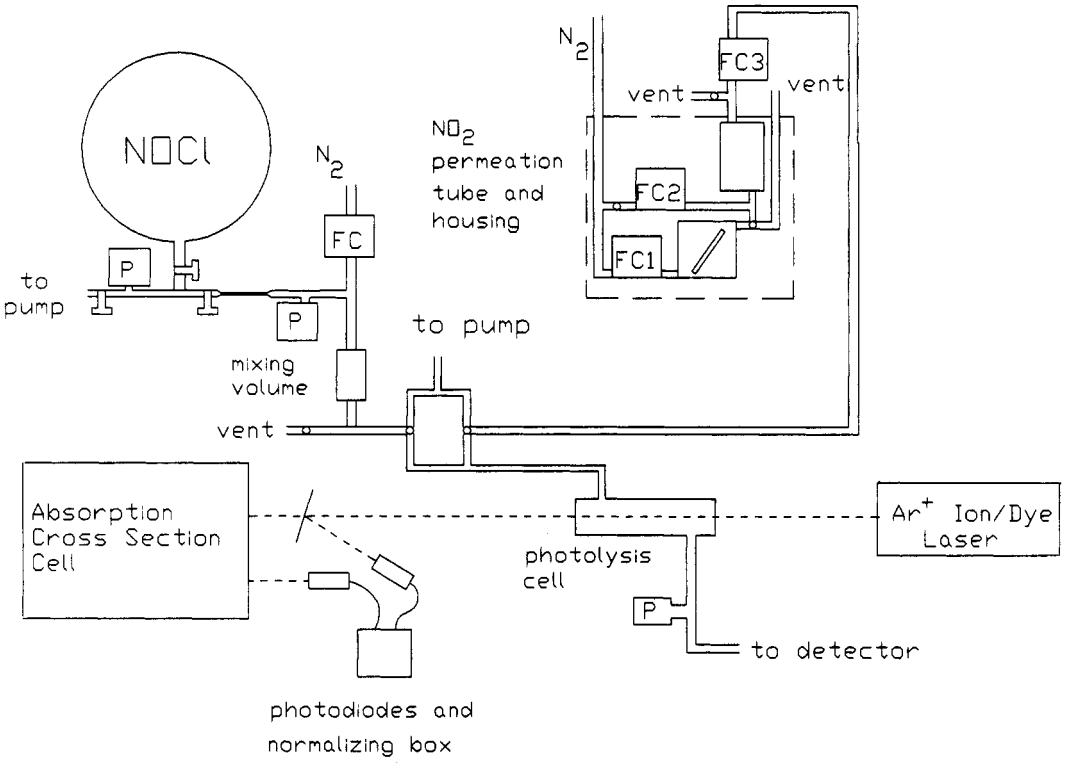


**Figure 1.** Schematic of the apparatus used in the measurement of $NO_2$ absorption cross sections and quantum yields. FC: flow controllers. P: pressure gauges.

It is clear that photodissociation beyond threshold occurs with the aid of rovibrational energy. This leads to the possibility that the structured nature of the $NO_2$ spectrum may actually manifest itself in the wavelength dependence of the quantum yield measurements, since the internal energy content of the $NO_2$ may be significantly different at a peak in the absorption spectrum compared to a nearby valley.

In this work, we present new contributions to the $NO_2$ photolysis picture. $NO_2$ cross section and quantum yield measurements are made at very high resolution (0.001 nm) as a function of both temperature and wavelength. The goals of the work are as follows: to confirm the wavelength dependence of the $NO_2$ quantum yield data at room temperature, to provide a full set of low-temperature quantum yield data beyond the thermodynamic threshold, to determine the influence of the structured nature of the $NO_2$ absorption spectrum on the quantum yield, and finally, to explain quantitatively the mechanism involved in the photodissociation process in the energy-deficient region beyond 400 nm.

## Experimental Design

The general experimental procedure is as follows. $NO_2$ was photolyzed with the output of a dye laser system, and the NO formed in the photolysis was measured. NOCl, for which the quantum yield and absorption cross sections are known, was photolyzed under identical conditions, and the NO product was also measured in order to normalize for the laser power. The $NO_2$ absorption cross section was measured immediately before and/or after each photolysis experiment using the dye laser as the light source. The measured NO yields and absorption cross section were used to determine the $NO_2$ quantum yield as a function of temperature and wavelength. The setup for both the $NO_2$ photolysis and the absorption cross section experiments is shown schematically in Figure 1 and will now be discussed in detail.

For both the absorption cross section and quantum yield experiments, the output of a Coherent I-100 Argon Ion laser (all UV lines) was used to pump a ring dye laser (Coherent CR-699). The dye laser was operated with the three-plate birefringent filter in place, yielding a spectral resolution of ≈0.001 nm at 400 nm. Exalite 392 dye was used for wavelengths between 388 and 402 nm, Exalite 400 was used for wavelengths between 396 and 406 nm, and Stilbene 3 was used between 404 and 411 nm. A 30 cm monochromator and/or a wavemeter (Burleigh Model WA-2000S) were used to determine the laser wavelength to an accuracy of ±0.1 nm. The monochromator was calibrated using the lines from a low-pressure Hg lamp, while the wavemeter was calibrated with a He–Ne laser. Dye laser power ranged between 50 and 300 mW, depending on the wavelength and the age of the dye batch.

$NO_2$ absorption cross section experiments were conducted in a 1 meter long, temperature-controlled, stainless steel cell. The cell consisted of three concentric tubes, the innermost of which contained the $NO_2$ sample gas. The middle chamber contained the temperature-regulating fluid which was circulated from a temperature-controlled bath, and the outermost chamber served as an insulating dewar. Ethanol was used as the circulating fluid in these studies, and measurements were taken at both 248 and 298 K. Three Al–UV-coated mirrors were positioned (two on the back wall and one on the front wall directly between the windows) inside the innermost cell. The dye laser beam was passed into the absorption cell and made four passes through it, yielding an optical path of 4 m. Upon exiting the cell, the light was focused onto a 5.8 × 5.8 mm silicon photodiode, which was housed in a black anodized mount. A bandpass filter (nominally centered at 400 ± 3.5 nm with a band width of 25 ± 3.5 nm) was located at the opening of the housing to eliminate any contribution from room light. A series of black velvet anodized baffles lined the tubing leading to the photodiode to reduce scattered light. A quartz plano convex lens, placed immediately in front of the photodiode, focused the light onto the head of the diode. Neutral density filters were occasionally positioned in the housing as well, to avoid saturation of the photodiode and associated amplifiers. A portion of the incoming laser beam (~5%) was split off onto a second photodiode in order to monitor changes in the laser power between measurements of the reference and signal intensity.

Absorption cross sections were measured as follows. First, a reference signal ($I_0$) was measured at the wavelength of interest with the cell evacuated. Then, the cell was filled with $NO_2$ to pressures of 0.05–0.2 Torr. The $NO_2$ pressure and signal ($I$) were recorded. Several cross section measurements were taken by this method at a particular wavelength and temperature, and the absorption cross sections were determined using the Beer–Lambert law:

$$\sigma(\lambda,T) = \ln[I_0(\lambda,T)/I(\lambda,T)]/lc \qquad (C)$$

where $\sigma(\lambda,T)$ is the absorption cross section in $cm^2$ $molecule^{-1}$, $l$ is the pathlength in cm, and $c$ is the $NO_2$ concentration in molecule $cm^{-3}$. Cross sections were obtained from a linear least squares fit of $\ln[I_0(\lambda,T)/I(\lambda,T)]/l$ versus $c$. $NO_2$ absorption cross section measurements were made immediately before or after every photolysis measurement to ensure that both the cross section and quantum yield measurements were made at the same laser wavelength. This procedure was necessary due to the structured nature of the $NO_2$ absorption spectrum and the high resolution of the photolysis laser.

The $NO_2$ quantum yield experiment consisted of five main components: a flowing $NO_2$ inlet system, a flowing NOCl inlet system, an NO chemiluminescence detector, the argon ion/dye laser system with associated optics and photodiodes, and an IBM XT computer. The flowing $NO_2$ mixture was generated by passing a known flow (normally ~40 standard $cm^3$/min or sccm) of ultrahigh purity (UHP) nitrogen over an $NO_2$ permeation vial (Thermedics Inc.). The permeation tube dilution system was maintained at 30 ± 1.5 °C in a temperature-regulated housing. The $NO_2$ mixture was further diluted with UHP $N_2$ such that concentrations were several parts per million by volume (ppmv). A total of 400 sccm of the diluted $NO_2$ mixture was passed into the photolysis cell through a flow controller, while the remaining flow was vented.

Nitrosyl chloride, NOCl, was employed as an actinometer in the $NO_2$ photolysis experiments. NOCl was synthesized and purified from the reaction of NO with $Cl_2$[47] and its purity determined by Fourier transform IR spectroscopy. Small amounts of NO, <0.5%, and $NO_2$, <0.1%, were typically present after purification. The presence of NO impurity has no effect on the experimental results, except to contribute a background signal in the chemiluminescence detector. The presence of $NO_2$ was potentially a larger problem, since the absorption cross section of $NO_2$ is some 10–15 times larger than that of NOCl in the wavelength range studied here. Hence, photolysis of $NO_2$ impurity could contribute significantly to the observed NO signal during NOCl photolysis experiments. At the 0.1% impurity level, however, this effect was less than 2% in all the experiments conducted here. The NOCl was transferred into a 22 L darkened bulb and was diluted with UHP nitrogen such that the mixing ratio of NOCl was $(1–2) \times 10^{-3}$. The absolute NOCl concentration in the bulb was determined using infrared spectroscopy.

For the flowing NOCl system, glass and Teflon valves and Galtek (Teflon) connections were used wherever possible, as NOCl was found to decompose on stainless steel. Glassware was either blackened or covered with black felt to eliminate NOCl decomposition in room light. A glass capillary flowing system was employed rather than a mass flow controller to avoid contact of the NOCl with metal surfaces. The NOCl mixture was diluted with a known flow of UHP $N_2$ once beyond the capillary system, resulting in mixing ratios of 1–5 ppm. A major portion of the total flow was vented, while the remainder (~400 sccm) was directed into the photolysis cell.

In order to facilitate alternate $NO_2$/NOCl photolysis measurements, a system of three-way solenoid valves was employed so that both the $NO_2$ and NOCl flowing systems could be operative simultaneously, yet separately, as shown in Figure 1. One gas was directed through the photolysis cell, while the other was directed to a pump. The photolysis cell consisted of three concentric glass cells. The gas sample passed through the innermost cell. This portion of the cell was 20 cm long with an inner diameter of 2.5 cm. The middle cell contained the circulating temperature bath fluid, again ethanol. The temperature of the ethanol was regulated by the same temperature bath as was used for the cross section measurements. Data were collected at 248 and 298 K. The outermost jacket of the cell was evacuated for insulative purposes.

Photolysis measurements were made by passing the laser beam through the photolysis cell through which either $NO_2$ or NOCl was flowing and monitoring the NO product formed. Alternate $NO_2$/NOCl photolysis measurements were carried out at each wavelength and temperature studied. A photodiode, placed after the photolysis cell, measured relative laser power. The photolysis signals could thus be corrected for changes in the laser power between measurements. Gas concentrations and residence times in the photolysis cell were kept low to minimize the effects of secondary chemistry. Between 5–20% of the $NO_2$ and 0.5–2.5% of the NOCl were converted to NO for most experiments. Residence times in the cell were on the order of 2–4 s. Typical flows were ≈400 sccm, and cell pressures were between 150 and 300 Torr.

An NO chemiluminescence detector was employed to determine amounts of NO formed during the photolysis experiments, as well as amounts of $NO_2$ and NOCl sample gases. The NO detector makes use of the high sensitivity of the chemiluminescence reaction

$$NO + O_3 \rightarrow NO_2^* + O_2 \qquad (5)$$

where $NO_2^*$ refers to $NO_2$ in an excited electronic state which then fluoresces at $\lambda > 600$ nm. Ozone was added in excess to the flow of gas from the photolysis cells, thereby producing chemiluminescence proportional to the amount of NO in the gas sample. The photons produced in the reaction were monitored with an EMI 9658R photomultiplier tube, and the analog signals from a picoammeter were recorded. Although only relative NO amounts were actually used in calculating the $NO_2$ quantum yields, it was necessary to calibrate the detector in order to ensure its linearity. Calibrations were done using two NO standard mixes (1.6 and 9.13 ppm NO standards) which were dynamically diluted to between ~0.01 and 6 ppmv. The detector was linear over the range investigated. The effect of background gases on detector sensitivity was also explored. It was shown that the detector had essentially identical sensitivity to NO regardless of the concentration or identity of background gas (i.e. $N_2$, $NO_2$, or NOCl).

The relative amounts of $NO_2$ and NOCl present were determined by conversion to NO on a heated gold converter catalyst,[25] located in the sample line upstream of the detector. The NOCl or $NO_2$ gas was directed through this converter, along with ~2.5 sccm of $H_2$ carrier gas. Typical concentrations of $NO_2$ were ~1.5 ppm, while NOCl concentrations ranged from 1 to 5 ppm. Converter efficiencies for $NO_2$ were >95%. $NO_2$ concentrations measured with the converter agreed to within 5–10% with those calculated from known permeation rates and dilution flows.

A check on the converter efficiency for NOCl was done using a Xe arc lamp. The output of the lamp was passed through the photolysis cell with NOCl flowing through it, and the NO produced was recorded. Approximately one-third of the NOCl was dissociated using the lamp alone. Then, the lamp was turned off, the NOCl was directed through the converter, and the NO signal was again recorded. With the converter still on, the lamp was again turned on and no change in the NO signal was detected, indicating a converter efficiency of >95%.

A personal computer with a data acquisition and control board was interfaced to the experiment to acquire and store data from

the pressure transducers, photodiodes, and the chemiluminescence instrument, to operate solenoid valves and flow controllers, and to perform calculations.

**Results and Discussion**

In the wavelength range of interest to this study, $NO_2$ photolysis occurs as follows:

$$NO_2 + h\nu \rightarrow NO\ (X^2\Pi) + O(^3P) \quad (1)$$

In the absence of $O_2$, as was the case in most experiments, subsequent reaction of O with $NO_2$ produces a second NO molecule:

$$NO_2 + O \rightarrow NO + O_2 \quad (6)$$

Hence, the rate of production of NO is given by

$$d[NO]/dt = 2j_{NO2}[NO_2] = 2I_{NO2}\,\sigma_{NO2}\,\phi_{NO2}\,[NO_2] \quad (D)$$

where $j_{NO2}$ is the photolysis rate coefficient of $NO_2$, $I_{NO2}$ is the laser fluence, $\sigma_{NO2}$ is the $NO_2$ absorption cross section, and $\phi_{NO2}$ is the $NO_2$ photolysis quantum yield at wavelength $\lambda$. Integrating this expression yields

$$\phi_{NO_2}(\lambda) = \frac{-\ln\left(1-\frac{[NO]_t}{[NO_2]_o}\right)}{2I_{NO_2}(\lambda)\sigma_{NO_2}(\lambda)\,t} \quad (E)$$

Rather than relying on absolute measurements of residence time ($t$) and laser fluence ($I$) to determine $\phi_{NO2}$, we employed NOCl as an actinometer. The photochemistry of NOCl is well characterized in the spectral region of interest, and its quantum yield is known to be unity.[10] The choice of NOCl as actinometer was also advantageous in that the same NO chemiluminescence detector could be used for both NOCl and $NO_2$ photolysis measurements. In our system, NOCl photolysis occurs as follows:

$$NOCl + h\nu \rightarrow NO(X^2\Pi) + Cl(^2P) \quad (7)$$

$$Cl + NOCl \rightarrow NO + Cl_2 \quad (8)$$

By analogy to $NO_2$, $\phi_{NOCl}$ is given by the following equation:

$$\phi_{NOCl}(\lambda) = \frac{-\ln\left(1-\frac{[NO]_t}{[NOCl]_o}\right)}{2I_{NOCl}(\lambda)\sigma_{NOCl}(\lambda)\,t} \quad (F)$$

Finally, the ratio of these two equations yields the $NO_2$ quantum yield in terms of measured concentrations, flows, and pressures,

$$\phi_{NO_2}(\lambda) = \frac{-\ln\left(1-\frac{[NO]_t}{[NO_2]_o}\right)}{-\ln\left(1-\frac{[NO]_t}{[NOCl]_o}\right)} \frac{\sigma_{NOCl}}{\sigma_{NO_2}} \frac{P_{NOCl}}{P_{NO_2}} \frac{F_{NO_2}}{F_{NOCl}} \frac{I_{NOCl}}{I_{NO_2}} \quad (G)$$

where the measured flows and pressures in the photolysis cell are used to determine the relative residence time in the photolysis of $NO_2$ and NOCl. The temperature-dependent NOCl cross sections, $\sigma_{NOCl}$, were measured in a separate experiment.[47] Relative amounts of $NO_2$ and NOCl used in the photolysis experiments were determined by first converting to NO in the converter and then measuring the NO concentration with the chemiluminescence detector. The NO produced in the photolysis reactions was also measured with the chemiluminescence detector. Relative laser intensities were measured with the photodiode for each of the $NO_2$ and NOCl photolysis measurements to normalize for the small changes (typically less than 10%) in the laser power between measurements.

Several small corrections were made to account for secondary chemistry not considered above. At low pressures (<50 Torr), O atoms produced in the photolysis of $NO_2$ react almost exclusively with $NO_2$ via eq 6 to produce NO. However, at higher pressures and lower temperatures, the third body reaction

$$O + NO_2 + M \rightarrow NO_3 + M \quad (9)$$

becomes significant. The $NO_3$ produced in this reaction then reacts mainly with the photolysis product NO for the experimental conditions employed here,

$$NO_3 + NO \rightarrow 2NO_2 \quad (10)$$

leading to a lowering of the $NO_2$ to NO conversion rate. Computer simulations of the reaction system, using rate coefficient data of DeMore *et al.*,[48] were conducted to apply corrections to the measured NO at each of the pressures and temperatures studied. The amount of correction is approximately equal to the ratio of the rate constants for reactions 9 and 6 and was as little as 3% at 298 K and 150 Torr and as much as 12% at 248 K and 300 Torr.

$NO_2$ absorption cross sections required correction for $N_2O_4$ contributions at 248 K. The total concentration measured in each absorption cross section experiment is a sum of the $NO_2$ and $N_2O_4$ concentrations. The concentrations of $NO_2$ and $N_2O_4$ were determined using the $K_{eq}$ recommended by DeMore *et al.*:[48]

$$K_{eq}(248\cdot K) = [N_2O_4]/[NO_2]^2 = 2.1 \times 10^{-17}\ cm^3/molecule \quad (H)$$

The measured absorbance ($A$) is given by:

$$A/l = \sigma_{NO2}[NO_2] + \sigma_{N2O4}[N_2O_4] \quad (I)$$

From $N_2O_4$ cross sections of Bass *et al.*[38] near 400 nm, the absorption cross section for $NO_2$ ($\sigma_{NO2}$) was determined. Concentrations of $NO_2$ employed in the photolysis portion of the experiment were low enough to exclude significant formation of $N_2O_4$.

Uncertainties in the quantum yield calculations result from precision and/or possible systematic errors in the determination of each of the terms in eq G. Precision errors include ±4% for laser normalization, ±3% for $\sigma_{NOCl}$ and $\sigma_{NO2}$ measurements, ±2% for each NO determination, and ±1% for NOCl and $NO_2$ relative amounts and total flow determinations. Possible systematic errors include inefficient conversion of NOCl to NO in the converter (+5%), possible NO or $NO_2$ impurities in the NOCl sample which would raise the $\sigma_{NOCl}$ and hence raise the $NO_2$ quantum yield (±2%), and uncertainty in the rate coefficient data for reactions 6 and 9 (±2%). Combining the above factors yields a $2\sigma$ uncertainty of +15% and −10%.

$NO_2$ quantum yields measured at 298 K as a function of wavelength are plotted as the square symbols in Figure 2. The values average 0.93 (with an error of +15%/−10%) between 388 and 398 nm. The observation of quantum yields less than unity at photon energies greater than the photodissociation threshold has been reported previously (see ref 10 and references therein), although no explanation of this observation has been presented. The measured quantum yields then fall off smoothly at longer wavelengths to a value of 0.12 at 411 nm (the longest wavelength studied). Measured $NO_2$ absorption cross sections vary over the range $(4.7–6.8) \times 10^{-19}$ cm$^2$ molecule$^{-1}$ between 400 and 412 nm. However, no systematic variation is observed in the measured quantum yields with changes in the cross section; i.e., rovibrational structure in the $NO_2$ absorption spectrum appears to have no significant effect on the quantum yield over this wavelength range.

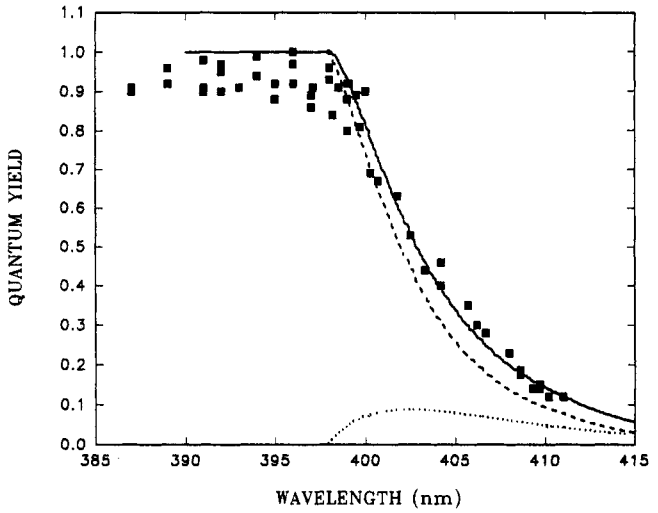


**Figure 2.** $NO_2$ quantum yields (■) obtained at 298 K as a function of wavelength. Also shown are curves showing calculated quantum yields due to internal energy (dashed line), the calculated dissociation due to collisions (dotted line), and the sum of these two calculations (solid line).

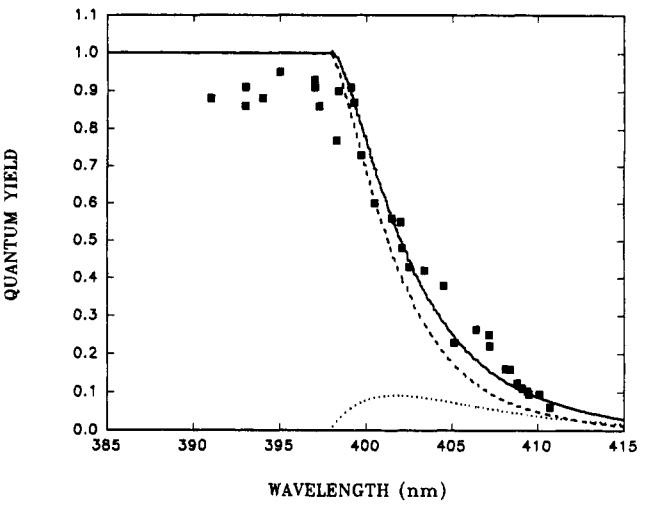


**Figure 3.** $NO_2$ quantum yields (■) obtained at 248 K as a function of wavelength. Also shown are curves showing calculated quantum yields due to internal energy (dashed line), the calculated dissociation due to collisions (dotted line), and the sum of these two calculations (solid line).

Current recommendations for $NO_2$ quantum yields at room temperature are taken from the evaluation of Gardner *et al.*,[10] who obtained a "best fit" of the corrected data of Harker *et al.*[8] (1977) for 397–420 nm, Davenport[9] (1978) for 400–420 nm, Jones and Bayes[6,12] (1971, 1973) for 297.6–412 nm (excluding data at 366.3 nm), and their work, for 334.1–404.3 nm. The data reported here are slightly lower (some 5% on average) than the recommendations between 388 and 397 nm, although the discrepancy is well within experimental uncertainty. However, it should be pointed out that, in arriving at the recommended values for this wavelength region, Gardner *et al.* excluded a number of quantum yield determinations significantly less than 1 that have been reported by other authors (e.g., Jones and Bayes,[6,12] Harker *et al.*,[8] Davenport,[9] and Gaedtke and Troe[7]).

In addition, the falloff at wavelengths above 398 nm observed here is not as rapid as that recommended by Gardner *et al.* The best estimates of Gardner *et al.* for the 398–402 nm region are based largely on the data of Harker *et al.*,[8] whose data below 397 nm were excluded by Gardner *et al.* because they were low in view of other more direct measurements. Hence it is possible that the Harker data near 400 nm are also too low and that this skews the Gardner *et al.* fit to lower values in the 398–402 nm range. Also, previous measurements were made at lower spectral resolutions, and it is possible that this leads to a broader falloff of quantum yield with wavelength relative to our work.

The 248 K data obtained in this work are shown as the square symbols in Figure 3. The data between 388 and 398 are slightly lower than the 298 K data and show no wavelength dependence. The average quantum yield is 0.90. The 248 K quantum yield data in the falloff region are systematically lower than the 298 K data, and the ratio of $\phi_{298}/\phi_{248}$ increases with increasing wavelength, from a value of 1.1 at 398 nm to 2.0 at 411 nm. Again, no significant correlation of quantum yield with cross section is apparent beyond 400 nm as the quantum yield falls off smoothly with wavelength.

Most previous low-temperature measurements of $NO_2$ quantum yields were conducted using the mercury line at 404.7 nm, and quantum yield values of 0.39 at 298 K and 0.29 at 248 K were obtained.[28] Although we made no measurements at exactly this wavelength, averaging the two nearest data points to 404.7 nm gives $\phi$ values of 0.41 at 298 K and 0.30 at 248 K, in excellent agreement with the previous data.

A number of test experiments were conducted to check for possible effects of secondary chemistry and two-photon processes. First, measurements were made at two different total pressures (150 and 300 Torr) with substantially no effect on the observed quantum yield, indicating that inaccuracies due to correction for reactions 9 and 10 were not significant. In addition, the effect of beam geometry (and hence of fluence) was investigated near 410 nm. A beam expander was placed in the laser path in front of the photolysis cell in several test measurements, increasing the beam diameter from its normal 4 mm to ~20 mm. Quantum yields measured both with and without the beam expander were essentially identical, indicating that no significant two-photon dissociation of $NO_2$ was occurring. Finally, test experiments were conducted using $O_2$ as the buffer gas rather than $N_2$. While this should have no effect on the NOCl system, the secondary reactions following $NO_2$ photolysis are different,

$$NO_2 + h\nu \rightarrow NO + O \quad (1)$$

$$O + O_2 \rightarrow O_3 \quad (11)$$

and only one NO is expected per $NO_2$ dissociated. Quantum yields obtained with $O_2$ as buffer gas were identical to those obtained in $N_2$, indicating that secondary chemistry involving the O atom is properly accounted for. This result also indicates that reaction of excited $NO_2$ with $O_2$, a reaction postulated by Zellner *et al.*,[49]

$$NO_2 + h\nu \rightarrow NO_2^*$$

$$NO_2^* + O_2 \rightarrow NO + O_3 \quad (12)$$

is not occurring under the conditions of this study and is unlikely to be of atmospheric relevance.

One of the primary motivations for this study was to address the issue of the mechanism of the photodissocation beyond the thermodynamic threshold. As discussed in the Introduction, theoretical treatments in which all of the rovibrational energy of $NO_2$ is employed to aid in the photodissociation lead to quantum yields that are significantly less than those observed experimentally. This result is confirmed in the present work, as displayed in Figures 2 and 3. The theoretical curves were obtained in a fashion identical to that previously employed.[14,28]

Clearly, there is another mechanism in operation which aids the dissociation of $NO_2$ molecules which are excited to energies just below threshold. We believe that this mechanism is collisional,[7] and a quantitative description of this model is now presented. Fluorescence lifetimes of $NO_2$ molecules just below the dissociation limit are anomolously long,[50] in the neighborhood of 50–100 $\mu$s, owing to the coupling between ground and excited

electronic states. Therefore, such molecules will be subject to collisions in experiments conducted at pressures of a few milliTorr or greater.

It is well established[7,51] that photon absorption near threshold promotes $NO_2$ to a region of strong mixing between the excited $^2B_2$ and the ground $^2A_1$ state. Hence, due to the large density of ground state levels, a photoexcited molecule can be characterized as an excited molecule with essentially ground electronic state character. Collisional energy transfer distributions for thermally excited $NO_2$ with bath gas molecules have been studied by Troe and co-workers,[7,52] and the following parameterization has been presented:

$$P(E,E') = \frac{1}{\alpha+\gamma}\exp\left(-\frac{E-\beta-E'}{\alpha}\right) \quad \text{for } E' \le E-\beta \quad \text{(J)}$$

$$P(E,E') = \frac{1}{\alpha+\gamma}\exp\left(-\frac{E'-E+\beta}{\gamma}\right) \quad \text{for } E' \ge E-\beta \quad \text{(K)}$$

where $P(E,E')$ is the collisional transition probability, $E$ and $E'$ are the energy before and after collision, and the values of $\alpha$, $\beta$, and $\gamma$ are selected as 540, 245, and 335 $cm^{-1}$, respectively.[7,52] The significant consequence of this result is that, although the average energy transfer per collision is $-450$ $cm^{-1}$ and deactivates the excited $NO_2$, a significant fraction of the $NO_2$ molecules (ca. 20%) are actually excited by collision. Since the dissociation lifetime for $NO_2$ just above the dissociation limit is a few picoseconds[50] (i.e., some 100 times shorter than the time between collisions at atmospheric pressure), an $NO_2$ molecule promoted by collision from just below the dissociation limit to above it will dissociate before it suffers further collisions. These enhanced quantum yields above the zero-pressure limit for wavelengths longer than 400 nm were originally predicted by Gaedtke and Troe (see their Figure 5).[7]

In order to estimate the contribution of this collisional uppumping to the predicted quantum yields, the following procedure was used. As in previous calculations, all molecules possessing sufficient internal rovibrational energy to overcome the dissociation barrier following excitation at wavelength $\lambda$ were assumed to dissociate. The remaining molecules were then subjected to a collision, and their energy was adjusted by the function given above. Any molecules promoted above the barrier following collision were then assumed to dissociate. The yields of molecules dissociating due to collision at 298 and 248 K are given in Figures 2 and 3. The total theoretical quantum yields are then obtained as the sums of those molecules that dissociate directly and those that dissociate with the aid of a collision. These total calculated quantum yields as a function of wavelength, shown in Figures 2 and 3, are in excellent agreement with the measurements at both 298 and 248 K. Recommended quantum yields at 248 and 298 K are given in Table 1; these recommendations are obtained from the measured data between 390 and 397 nm (where $\phi$ is measured to be constant) and from the theoretical functions for longer wavelengths.

## Conclusions

Quantum yields for the photodissociation of $NO_2$ have been measured as a function of wavelength at two temperatures (248 and 298 K). The room temperature data, although measured at higher spectral resolution, are in good accord with previous data with the exception that the falloff in quantum yield occurs at longer wavelength than currently recommended. This work represents the first measurement of low-temperature $NO_2$ quantum yields throughout the entire falloff region. The 248 K data are found to be significantly lower than the 298 K data between 398 and 411 nm, the difference being about a factor of 2 near 411 nm.

**TABLE 1: Recommended $NO_2$ Quantum Yields vs Wavelength at 298 and 248 K**

| wavelength (nm) | quantum yield at 298 K | quantum yield at 248 K |
|---|---|---|
| 390–397 | 0.93 | 0.90 |
| 398 | 0.90 | 0.87 |
| 399 | 0.88 | 0.85 |
| 400 | 0.82 | 0.77 |
| 401 | 0.70 | 0.62 |
| 402 | 0.58 | 0.50 |
| 403 | 0.49 | 0.40 |
| 404 | 0.41 | 0.31 |
| 405 | 0.34 | 0.25 |
| 406 | 0.28 | 0.20 |
| 407 | 0.24 | 0.16 |
| 408 | 0.20 | 0.13 |
| 409 | 0.17 | 0.11 |
| 410 | 0.14 | 0.09 |
| 411 | 0.12 | 0.07 |
| 412 | 0.10 | 0.06 |
| 413 | 0.08 | 0.05 |
| 414 | 0.07 | 0.04 |
| 415 | 0.06 | 0.03 |
| 416 | 0.05 | 0.02 |
| 417 | 0.04 | 0.02 |
| 418 | 0.03 | 0.02 |
| 419 | 0.02 | 0.01 |
| 420 | 0.02 | 0.01 |
| 422 | 0.01 | 0.01 |
| 424 | 0.01 | 0.01 |
| 426 | 0.01 | 0.00 |
| 428 | 0.01 | 0.00 |

Finally, the mechanism of photodissociation beyond the thermodynamic threshold has been quantitatively explained. Dissociation beyond threshold occurs predominantly with the aid of rovibrational energy, as was reported previously. Additional $NO_2$ photodissociation appears to occur as a result of collisions of $NO_2$ molecules excited to near the energy barrier with bath gas molecules. There appears to be no contribution of rovibrational structure in the $NO_2$ spectrum to the observed wavelength dependence of the quantum yield data.

**Acknowledgment.** This work was supported in part by a grant from the NASA Upper Atmosphere Research Program (Contract W-16042). The National Center for Atmospheric Research is supported by the National Science Foundation. C.M.R. and G.J.V. acknowledge the receipt of fellowships from the NCAR Advanced Study Program. This work makes up a part of the Ph.D. thesis of C.M.R. NCAR Cooperative Thesis No. 133, 1992.

**Note Added in Proof.** Bieler *et al.* (*J. Phys. Chem.* **1994**, *98*, 1058) recently demonstrated the collision-induced dissociation of $NO_2$ molecules excited to just below the threshold in a crossed-beam experiment.

## References and Notes

(1) Dickinson, R. G.; Baxter, W. P. *J. Am. Chem. Soc.* **1928**, *50*, 774.
(2) Norrish, R. G. W. *J. Chem. Soc.* **1929**, 1158.
(3) Holmes, H. H.; Daniels, F. *J. Am. Chem. Soc.* **1934**, *56*, 630.
(4) Blacet, F. E.; Hall, T. C.; Leighton, P. A. *J. Am. Chem. Soc.* **1962**, *84*, 4011.
(5) Pitts, J. N., Jr.; Sharp, J. H.; Chan, S. I. *J. Chem. Phys.* **1964**, *42*, 3655.
(6) Jones, I. T. N.; Bayes, K. D. *J. Chem. Phys.* **1973**, *59*, 4836.
(7) Gaedtke, H.; Troe, J. *Ber. Bunsen-Ges. Phys. Chem.* **1975**, *79*, 184.
(8) Harker, A. B.; Ho, W.; Ratto, J. J. *Chem. Phys. Lett.* **1977**, *50*, 394.
(9) Davenport, J. E. *FAA-Eq-78-14*, **1978**, High-Altitude Prog., Off. of Environ. Qual., Fed. Avia. Admin.: Washington, D.C., 1978.
(10) Gardner, E. P.; Sperry, P. D.; Calvert, J. G. *J. Geophys. Res.* **1987**, *92*, 6642.
(11) Troe, J. *Ber. Bunsen-Ges. Phys. Chem.* **1969**, *73*, 906.
(12) Jones, I. T. N.; Bayes, K. D. *Chem. Phys. Lett.* **1971**, *11*, 163.
(13) Gaedtke, H.; Hippler, H.; Troe, J. *Chem. Phys. Lett.* **1972**, *16*, 177.
(14) Lee, E. K. C.; Uselman, W. M. *Faraday Discuss., Chem. Soc.* **1972**, *53*, 125.

(15) Jones, I. T. N.; Bayes, K. D. *J. Chem. Phys.* **1973**, *59*, 3119.
(16) Hakala, D.; Harteck, P.; Reeves, R. R. *J. Phys. Chem.* **1974**, *78*, 1583.
(17) Demerjian, K. L; Kerr, J. A.; Calvert, J. G. *Adv. Environ. Sci. Technol.* **1974**, *4*, 1.
(18) Hippler, H.; Schippert, C.; Troe, J. *Int. J. Chem. Kinet., Symp.* **1975**, *1*, 27.
(19) Creel, C. L.; Ross, J. *J. Chem. Phys.* **1976**, *64*, 3560.
(20) Demerjian, K. L.; Schere, K. L.; Peterson, J. T. *Adv. Environ. Sci. Technol.* **1980**, *10*, 369.
(21) Dickerson, R. R.; Stedman, D. H.; Delany, A. C. *J. Geophys. Res.* **1982**, *87*, 4933.
(22) Parrish, D. D.; Murphy, P. C.; Albritton, D. L.; Fehsenfeld, F. C. *Atmos. Environ.* **1983**, *17*, 1365.
(23) Madronich, S. *Atmos. Environ.* **1987**, *21*, 569.
(24) Shetter, R. E.; Davidson, J. A.; Cantrell, C. A.; Burzynski, N. J., Jr.; Calvert, J. G. *J. Geophys. Res.* **1988**, *93*, 7113.
(25) Shetter, R. E.; McDaniel, A. H.; Cantrell, C. A.; Madronich, S.; Calvert, J. G. *J. Geophys. Res.* **1992**, *97*, 10349.
(26) Douglas, A. E.; Huber, K. P. *Can. J. Phys.* **1965**, *43*, 74.
(27) Uselman, W. M.; Lee, E. K. C. *J. Chem. Phys.* **1976**, *64*, 3457.
(28) Calvert, J. G.; Madronich, S.; Gardner, E. P.; Davidson, J. A.; Cantrell, C. A.; Shetter, R. E. *J. Phys. Chem.* **1987**, *91*, 6339.
(29) Davidson, J. A.; Cantrell, C. A.; McDaniel, A. H.; Shetter, R. E.; Madronich, S.; Calvert, J. G. *J. Geophys. Res.* **1988**, *93*, 7105.
(30) Harris, L. *Proc. Nat. Acad. Sci. U.S.A.* **1928**, *14*, 690.
(31) Hermann, A. *Ann. Phys. 5 Folge* **1932**, *15*, 89.
(32) Harris, L.; King, G. W. *J. Chem. Phys.* **1940**, *8*, 775.
(33) Harris, L.; King, G. W.; Benedict, W. S.; Pearse, R. W. B. *J. Chem. Phys.* **1940**, *8*, 765.
(34) Dixon, J. K. *J. Chem. Phys.* **1940**, *8*, 157.
(35) Hall, T. C., Jr.; Blacet, F. E. *J. Chem. Phys.* **1952**, *20*, 1745.
(36) Nakayama, T.; Kitamura, M. Y.; Watanabe, K. *J. Chem. Phys.* **1959**, *30*, 1180.
(37) Johnston, H. S.; Graham, R. *Can. J. Chem.* **1974**, *52*, 1415.
(38) Bass, A. M.; Ledford, A. E., Jr.; Laufer, A. H. *J. Res. Natl. Bur. Stand., Sect. A* **1976**, *80*, 143.
(39) Hicks, E.; Leroy, B.; Rigaud, P.; Jourdain, J.; LeBras, G. *J. Chim. Phys.* **1979**, *76*, 693.
(40) Hsu, D. K.; Monts, D. L.; Zare, R. N. *Spectral Atlas of Nitrogen Dioxide 5580–6480 Å*; Academic Press: New York, 1978.
(41) Uehara, K.; Sasada, H. *High Resolution Spectra Atlas of Nitrogen Dioxide 559–597 nm*, Series in Chemical Physics, *Vol. 41*; Springer: New York, 1985.
(42) Schneider, W.; Moortgat, G. K.; Tyndall, G. S.; Burrows, J. P. *J. Photochem. Photobiol. A. Chem.* **1987**, *40*, 195.
(43) Koffend, J. B.; Holloway, J. S.; Kwok, M. A.; Heidner, R. F., III. *Report SD-TR-87-46*; Space Division, Air Force Systems Command, Los Angeles, CA, 1987.
(44) Madronich, S.; Hastie, D. R.; Ridley, B. A.; Schiff, H. I. *J. Atmos. Chem.* **1983**, *1*, 3.
(45) Madronich, S.; Hastie, D. R.; Ridley, B. A.; Schiff, H. I. *J. Atmos. Chem.* **1984**, *1*, 151.
(46) Madronich, S.; Hastie, D. R.; Schiff, H. I.; Ridley, B. A. *J. Atmos. Chem.* **1985**, *3*, 233.
(47) Roehl, C. M.; Orlando, J. J.; Calvert, J. G. *J. Photochem., Photobiol. A: Chem.* **1992**, *69*, 1.
(48) DeMore, W. B.; Sander, S. P.; Golden, D. M.; Hampson, R. F.; Kurylo, M. J.; Howard, C. J.; Ravishankara, A. R.; Kolb, C. E.; Molina, M. J. *Chemical Kinetics and Photochemistry Data for Use in Stratospheric Modeling*, Eval. No. 10, (JPL Publ. 92-20, 1992).
(49) Zellner, R.; Hartmann, D.; Rosner, I. *Ber. Bunsen-Ges. Phys. Chem.* **1992**, *96*, 385.
(50) Patten, K. O., Jr.; Burley, J. D.; Johnston, H. S. *J. Phys. Chem.* **1990**, *94*, 7960.
(51) Brucker, G. A.; Ionov, S. I.; Chen, Y.; Wittig, C. *Chem. Phys. Lett.* **1992**, *194*, 301.
(52) Troe, J. *Ber. Bunsen-Ges. Phys. Chem.* **1973**, *77*, 665.